Journal of Solid State Chemistry 183 (2010) 2689–2694

Contents lists available at ScienceDirect

Journal of Solid State Chemistry

journal homepage: www.elsevier.com/locate/jssc

B-site ordered perovskite $LaSrMnNbO_6$: Synthesis, structure and antiferromagnetism

Tao Yang [a], Tyché Perkisas [b], Joke Hadermann [b], Mark Croft [c], Alexander Ignatov [d], Martha Greenblatt [a,*]

[a] Department of Chemistry and Chemical Biology, Rutgers, the State University of New Jersey, 610 Taylor Road, Piscataway, NJ 08854-8087, USA
[b] Electron Microscopy for Materials Research (EMAT), University of Antwerp, Groenenborgerlaan 171, 2020 Antwerp, Belgium
[c] Department of Physics and Astronomy, Rutgers, The State University of New Jersey, 136 Frelinghuysen Road, Piscataway, NJ 08854, USA
[d] Materials Science and Engineering Department, Rutgers University, Piscataway, NJ 08854, USA

ARTICLE INFO

Article history:
Received 9 August 2010
Received in revised form
27 August 2010
Accepted 31 August 2010
Available online 8 September 2010

Keywords:
Double perovskite
Manganese
Niobium
B-cation ordering
Antiferromagnetic

ABSTRACT

$LaSrMnNbO_6$ has been synthesized by high temperature solid state reaction under 1% H_2/Ar dynamic flow. The structure is determined by Rietveld refinement of the powder X-ray diffraction data. It crystallizes in the monoclinic space group $P2_1/n$ with the unit cell parameters: $a=5.69187(12)$, $b=5.74732(10)$, $c=8.07018(15)$ Å and $\beta=90.0504(29)^\circ$, which were also confirmed by electron diffraction. The Mn^{2+} and Nb^{5+} ions, whose valence states are confirmed by X-ray absorption near-edge spectroscopy, are almost completely ordered over the *B*-site ($<1\%$ inversion) of the perovskite structure due to the large differences of both cationic size (0.19 Å) and charge. The octahedral framework displays significant tilting distortion according to Glazer's tilt system $a^-b^-c^+$. Upon heating, $LaSrMnNbO_6$ decomposes at 690 °C under O_2 flow or at 775 °C in air. The magnetic susceptibility data indicate the presence of long-range antiferromagnetic ordering at $T_N=8$ K; the experimentally observed effective paramagnetic moment, $\mu_{eff}=5.76\ \mu_B$ for high spin Mn^{2+} ($3d^5$, $S=5/2$) is in good agreement with the calculated value ($\mu_{calcd}=5.92\ \mu_B$).

1. Introduction

Cation order–disorder plays a critical role in the control of the crystal structure and the properties of many complex perovskite-type oxides. Superconductivity, colossal magnetoresistance, ferroelectricity, multiferroic behavior, magnetic ordering, piezoelectricity, electronic or ionic conductivity strongly depend on the degree of order of the *A* and/or *B* sites. In contrast to the relatively few *A*-site-ordered perovskites, there are numerous examples of *B*-site-ordered systems. Cationic order at the *B*-site in $AA'BB'O_6$ so-called double perovskites, either at short or long range, is a recurrent phenomenon. Generally, a B/B' ordered distribution is stabilized when the *B* and B' cations differ significantly in charge and/or ionic size [1]. The 1:1 $AA'BB'O_6$ (or $A_2BB'O_6$) double perovskites are the most common *B*-site ordered perovskites. In those systems, the different cations occupy two different sub-lattices in a "rock salt" distribution, such that the *B*-cations are ordered along the [111] direction with an order vector 1/2[111]. In such *B*-site ordered transition metal perovskites with unpaired *d* electrons, the magnetic interactions are enhanced and magnetic ordering [ferromagnetic (FM) or antiferromagnetic (AFM)] is likely to occur.

d^0 cation displacement from the center of a regular octahedron in perovskites is known to lead to ferroelectricity. The origin of such distortions is the second-order Jahn–Teller (SOJT) effect [2]. The SOJT distortion increases with decreasing energy difference between the metal empty *nd*-orbitals and the oxygen filled 2*p*-orbitals, which leads to a mixing of the corresponding metal and oxygen orbitals. The intrinsic displacement tendency of a given cation to distort its oxygen octahedra plays a critical role in ferroelectric perovskites. Recently, out-of-center displacements in 750 octahedrally coordinated d^0 transition metal oxides have been examined with a continuous symmetry measures approach [3]. With this approach, it was shown that the magnitudes and directions of the displacements scale roughly with the electronegativity of the cation and that the Nb^{5+} ion is a moderate distorter.

We were motivated to synthesize and study the properties of $LaSrMnNbO_6$ perovskite to investigate the possibility of *B*-cation order and consequent ferro- or antiferromagnetism induced by the ordered Mn^{2+} (high spin d^5) ions and the possibility of ferroelectrically distorted $Nb^{5+}O_6$ octahedra coupled to the magnetically ordered sub-lattice resulting in multiferroic properties. To the best of our knowledge, $LaSrMnNbO_6$ was mentioned in Attfield's publications, but without the structure and property details presented there [4,5]. In this paper, we show that although there is 1:1 *B*-site order of Mn^{2+}/Nb^{5+}, and AF order at low

* Corresponding author.
E-mail addresses: martha@rutchem.rutgers.edu, greenblatt@rutchem.rutgers.edu (M. Greenblatt).

0022-4596/$ - see front matter © 2010 Published by Elsevier Inc.
doi:10.1016/j.jssc.2010.08.041

temperatures, the distortion of the NbO_6 octahedra is negligible and unlikely to lead to ferroelectricity at least at room temperature.

2. Experimental section

$LaSrMnNbO_6$ was synthesized as a yellow powder sample by high temperature solid state reaction. Stoichiometric amounts of La_2O_3 (obtained by the dehydration of $La(NO_3)_3 \cdot 6H_2O$ at 800 °C), $SrCO_3$ (Aldrich, 99.995%), Mn_2O_3 (Aldrich, 99.999%) and Nb_2O_5 (Alfa, 99.9985%) were ground thoroughly using an agate mortar, pressed into a pellet and heated up to 1000 °C under 1% H_2/Ar dynamic flow for 12 h. After the pre-reaction, the sample pellet was further annealed at 1275 °C under 1% H_2/Ar dynamic flow for 120 h with several intermediate regrinding to obtain a pure and well crystallized sample. It should be noted that the 1% H_2/Ar flow should be dried with desiccant before flowing through the sample. The temperature window to synthesize $LaSrMnNbO_6$ is around 1250–1300 °C.

The purity of the product was confirmed by powder X-ray diffraction (PXD), which indicated no visible impurity reflection peaks. PXD data were recorded on a Bruker D8-Advance diffractometer (in Bragg–Brentano geometry with Cu$K\alpha$ radiation $\lambda = 1.5406$ Å, SOL-X solid state detector, 40 kV and 40 mA, step scan 10–120°/0.02°/15 s). The refinement of the crystal structure from PXD data was performed by the Rietveld method with the TOPAS software [6]. Samples for electron microscopy were prepared by dispersing the powder in ethanol and depositing it on a holey carbon grid. Energy dispersive X-ray (EDX) analysis was performed using a JEOL 5510 scanning electron microscope equipped with the Oxford INCA system. Electron diffraction (ED) patterns were obtained on a Philips CM20 transmission electron microscope. The Mn and Nb X-ray absorption near-edge spectroscopy data (XAS) were collected simultaneously in both the transmission and fluorescence mode on powder samples on beam line X-19A at the Brookhaven National Synchrotron Light Source. The thermal stability was analyzed with the combined thermogravimetric analysis (TGA) and differential scanning calorimetry (DTA) on a SDT Q600 thermogravimetric analyzer, in both air and O_2 atmosphere with a heating rate of 5 °C/min from 30 to 1100 °C. The *dc* magnetic susceptibility measurements were carried out on powder samples with a Quantum Design MPMS-XL superconducting quantum interference device (SQUID) magnetometer. Powder samples were placed in a gelatin capsule fastened in a plastic straw for immersion into the SQUID. Typical zero filed cooling (ZFC) and field cooling (FC) magnetizations in the temperature range of 5–300 K were performed under external fields of both 1 and 10 kOe. The isothermal magnetization curve was measured at 5 K up to 50 kOe.

3. Results and discussion

EDX measurements were performed on 105 different positions (Table S1 and Fig. S1 in the Supporting Information). The deduced formula, $La_{1.0(1)}Sr_{1.0(1)}Mn_{0.9(2)}Nb_{1.1(2)}O_6$, is in good agreement with the nominal stoichiometry within the experimental error. The results are concentrated around the nominal composition, which suggests good homogeneity of the compound.

The PXD pattern of $LaSrMnNbO_6$ is obviously much more complex than a simple cubic symmetry (Fig. 1). It can be indexed with a monoclinic unit cell $a \sim 5.69$, $b \sim 5.74$, $c \sim 8.07$ Å and $\beta \sim 90°$. Usually, the $\sim\sqrt{2}a_p \times \sqrt{2}a_p \times 2a_p$ unit cell is related to *Pbnm* or $P2_1/n$ for perovskites, and corresponds to a disordered or ordered perovskite model, respectively. Because $P2_1/n$ is a maximal non-isomorphic subgroup of *Pbnm*, it could be difficult to distinguish between these two space groups, especially if the ordering is

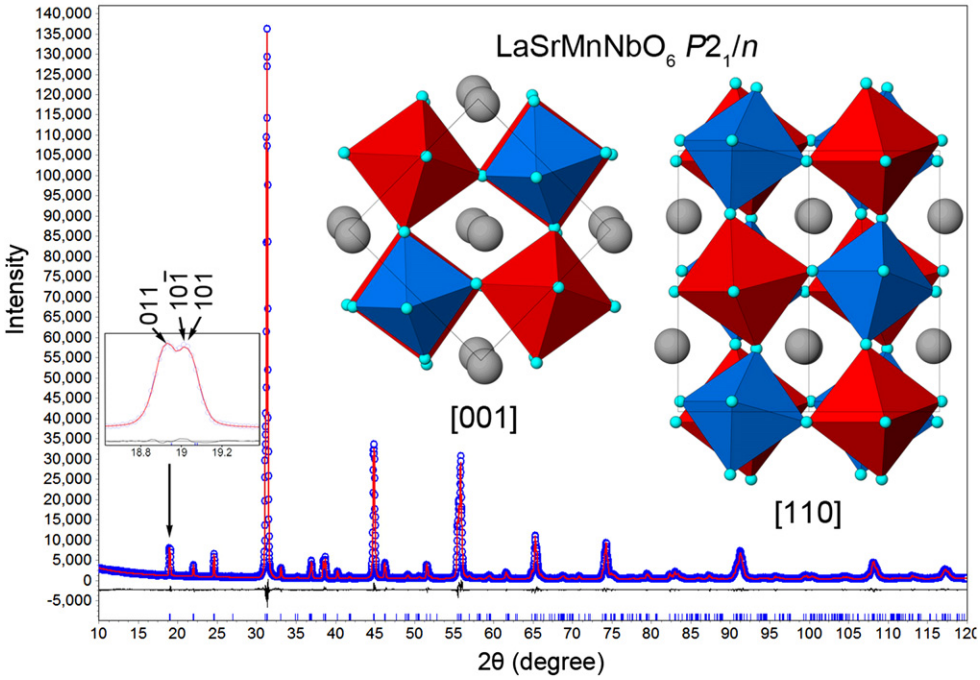

Fig. 1. Rietveld refinement of the PXD pattern for $LaSrMnNbO_6$. The blue symbol (○) represents the observed pattern and the red solid line is the calculated pattern; the blue marks below the diffraction patterns are the expected reflection positions, and the difference curve is also shown in black below the diffraction pattern. The left inset is the enlargement of the low-2θ diffractions. Structure views along the [010] and [110] directions are shown. (For interpretation of the references to colour in this figure legend, the reader is referred to the web version of this article.)

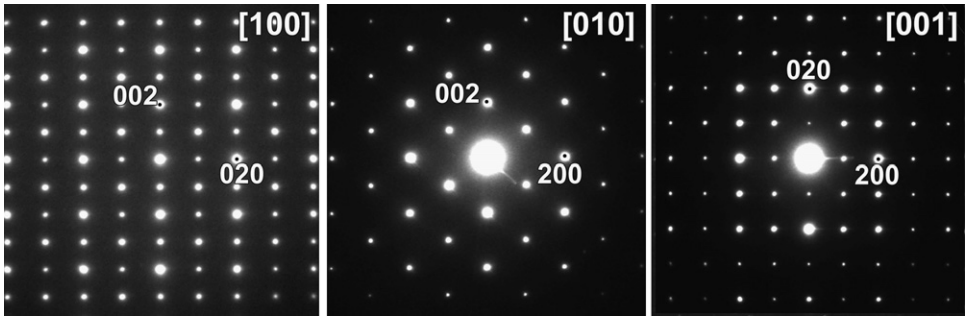

Fig. 2. Electron diffraction patterns on three main zones indexed in the general monoclinic unit cell: $\sim\sqrt{2}a_p \times \sqrt{2}a_p \times 2a_p$.

Table 1
Crystallographic and refined parameters of $LaSrMnNbO_6$.

Chemical formula	$LaSrMnNbO_6$
M_r (g mol^{-1})	470.38
Crystal system, space group	Monoclinic, $P2_1/n$
Temperature (K)	293
a (Å)	5.69187(12)
b (Å)	5.74732(10)
c (Å)	8.07018(15)
β (deg)	90.0504(29)
V (Å^3)	263.9997(88)
Z	2
ρ (g m^{-3})	5.919
Radiation type	Cu$K\alpha$ λ=1.5418 Å
Diffractometer	Bruker D8-Advance
Data collection mode	Reflection
Scan method	Step
2θ values (deg)	$2\theta_{min}$=10, $2\theta_{max}$=120, $2\theta_{step}$=0.02
R factors and goodness of fit	R_p=0.051, R_{wp}=0.072, R_{exp}=0.026, gof=2.73
Number of data points	5501
Number of parameters	43
Number of restraints	5

Table 2
Atomic coordinates and thermal displacement parameters for $LaSrMnNbO_6$ from room temperature PXD Rietveld refinement.

Atom	Position	x	y	z	U_{eq} (Å^2)	Occupancy	BVS
La	4g	0.0073(4)	0.0367(1)	0.2513(2)	0.0090(4)	0.5	2.38
Sr						0.5	2.06
Mn1	2d	0.5	0	0	0.0030(9)	0.998(7)	2.25
Nb1						0.002(7)	3.24
Mn2	2a	0.5	0	0.5	0.0037(6)	0.001(7)	3.47
Nb2						0.999(7)	4.99
O1	4g	0.280(2)	0.308(2)	0.040(2)	0.003(1)	1	
O2	4g	0.205(2)	0.779(2)	0.040(2)	0.003(1)	1	
O3	4g	0.081(2)	0.5199(8)	0.759(2)	0.003(1)	1	

incomplete and β is very close to 90°. The systematic refection conditions for *Pbnm* and $P2_1/n$ are identical with the exception that 0kl; k=2n reflections (e.g. 011) are allowed in $P2_1/n$, which is an indication of cation ordering [7]. The splitting of (011), (10−1) and (101) peaks is evident in Fig. 1, and thus the possibility of *Pbnm* is excluded. Electron diffraction was performed to confirm the unit cell dimensions and the space group. The electron diffraction patterns along the three main zones (Fig. 2) are consistent with the cell lattice of $\sim\sqrt{2}a_p \times \sqrt{2}a_p \times 2a_p$, and show reflection conditions $h\,k\,l$: no conditions, $h\,0\,l$: $h+l=2n$ and $0\,k\,0$:$k=2n$. This set of reflection conditions corresponds to only one possible space group, $P2_1/n$. Note that in Fig. 1 the reflections $0\,k\,0$: $k=2n+1$ are present, but when rotating the crystal around the b^*-axis, these reflections disappear as soon as the double diffraction paths are eliminated. This proves that they are due to double diffraction and are effectively forbidden reflections.

Rietveld refinement (Fig. 1) of the laboratory PXD data was thus carried out in the monoclinic space group $P2_1/n$. The refined parameters are listed in Table 1. Atomic coordinates and selected bond distances and angles are given in Tables 2 and 3. One feature of the double perovskites is that each material exhibits a unique tilt system. Space group $P2_1/n$ is commonly found for 1:1 rock-salt type B-cation ordering, with the 3-tilt system $a^-b^-c^+$ according to Glazer's notation [8]. The crystal structure of $LaSrMnNbO_6$ is shown along the [001] and [110] directions (inset of Fig. 1), where the in-phase and out-of-phase tilting can be clearly seen. The Rietveld refinement indicates nearly complete ordering (with $<1\%$ inversion) of Mn^{2+} and Nb^{5+} at the B-site.

The chemical shift of the Mn-K edge has been widely used to chronicle the evolution of the Mn valence state in oxide-based materials [9–13]. In Fig. 3a, the Mn-K edge of $LaSrMnNbO_6$ is compared to those of a series of Mn-standards. The well-known chemical shift of the Mn absorption edge to higher energy, with increasing formal oxidation state can clearly be seen by comparing the standard spectra for: the Mn^{2+} MnO, and Sr_2ReMnO_6 compounds; the Mn^{3+} $LaMnO_3$ compound; and the Mn^{4+} $CaMnO_3$ compound. The position of the $LaSrMnNbO_6$ spectrum close to the double perovskite Mn^{2+}, Sr_2ReMnO_6 standard spectrum clearly indicates a Mn^{2+} state in the former.

The intense peak features at the L_3-edges of 4d transition metals involve 2p-core to 4d final-state transitions [13–19]. These features can provide a probe of the empty 4d state energy distribution, albeit modified by the transition matrix element, core–hole interaction and multiplet effects [13–19]. In the top of Fig. 3b, the Nb-L_3-edges of a series of Nb-standard compounds are shown. The two perovskite based Nb^{5+} compounds display a robust, resolved two-peak structure with the lower energy peak (A) involving transitions into 4d-t_{2g} final states; and the high-energy peak (B) involving excitations into 4d-e_g states. The Nb^{5+}case is similar to Mo^{6+} compounds studied by our group in the past, where the 4d orbitals are empty [14–16,19]. As in the case of Mn, discussed above, a decreasing Nb valence (increasing 4d-electron count) would lead to a chemical shift of the absorption edge to lower energy. The chemical shift to lower energy from the Nb^{5+} perovskite standards to $Nb^{4+}O_2$ and still further to elemental-Nb can also be seen in Fig. 3b. Since the A-feature intensity is proportional to the number of 4d holes in the t_{2g} orbital a decreasing Nb

Table 3
Selected bond distances (Å) and angles (deg) in $LaSrMnNbO_6$.

Bond	Length	Bond	Length	Bond	Angle
La/Sr–O3	2.451(9)	Mn1/Nb1–O2(×2)	2.13(1)	O2–Mn1/Nb1–O3	90.5(5)
La/Sr–O1	2.46(1)	Mn1/Nb1–O3(×2)	2.14(1)	O2–Mn1/Nb1–O3	89.5(5)
La/Sr–O2	2.53(1)	Mn1/Nb1–O1(×2)	2.19(1)	O1–Mn1/Nb1–O2	88.8(5)
La/Sr–O3	2.598(5)	⟨Mn1/Nb1–O⟩	2.15	O1–Mn1/Nb1–O2	91.2(5)
La/Sr–O2	2.73(1)			O1–Mn1/Nb1–O3	89.5(4)
La/Sr–O1	2.78(1)			O1–Mn1/Nb1–O3	90.5(4)
La/Sr–O1	2.81(2)	Mn2/Nb2–O1(×2)	1.97(1)	O1–Mn2/Nb2–O3	90.3(5)
La/Sr–O2	2.84(2)	Mn2/Nb2–O3(×2)	2.00(1)	O1–Mn2/Nb2–O3	89.7(5)
⟨La/Sr–O⟩	2.65	Mn2/Nb2–O2(×2)	2.01(1)	O1–Mn2/Nb2–O2	91.4(5)
		⟨Mn2/Nb2–O⟩	1.99	O1–Mn2/Nb2–O2	88.6(5)
				O2–Mn2/Nb2–O3	87.2(3)
				O2–Mn2/Nb2–O3	92.8(3)
				Mn–O1–Nb	153.23°
				Mn–O2–Nb	155.60°
				Mn–O3–Nb	153.56°

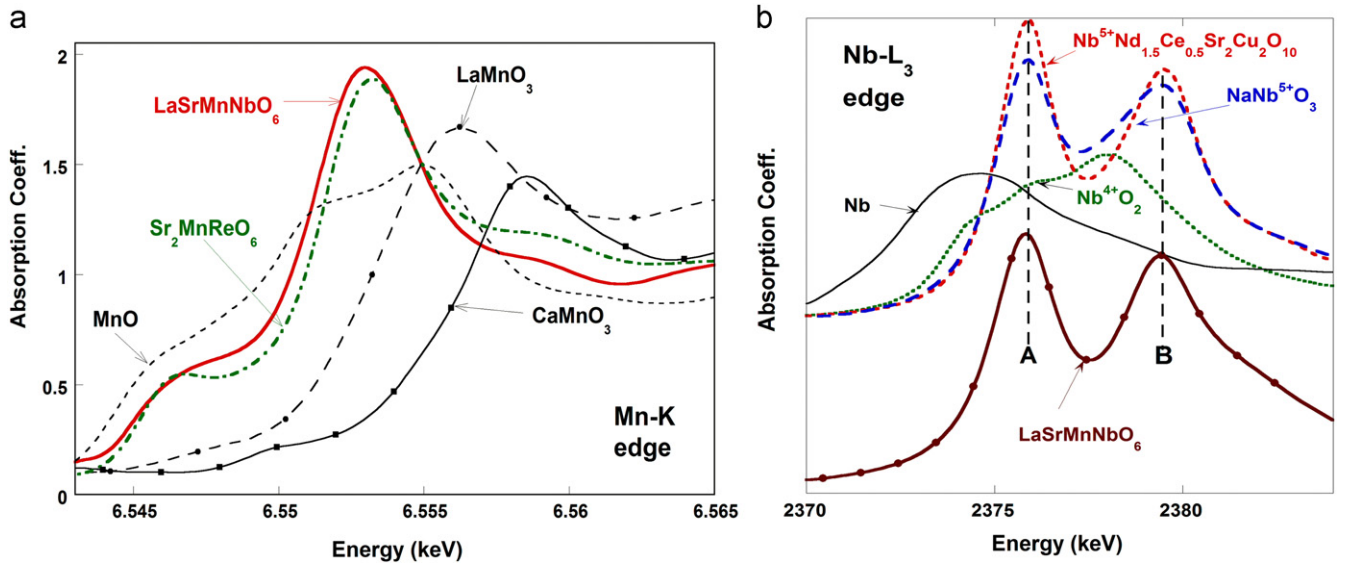

Fig. 3. (a) Mn-K edge XAS spectra for $LaSrMnNbO_6$ and the standards $Mn^{2+}O$, $Sr_2ReMn^{2+}O_6$, $LaMn^{3+}O_3$, $CaMn^{4+}O_3$ and (b) Nb-L_3 edge XAS spectra with the standards Nb, $Nb^{4+}O_2$, $NaNb^{5+}O_3$ and $Nb^{5+}Nd_{1.5}Ce_{0.5}Sr_2Cu_2O_{10}$.

valence (increasing 4*d*-electron count) would also lead to a decrease in the A-feature intensity. Such an A-feature degradation and chemical shift has been reported in multiple Mo-based compounds [14–16,19] and Ru compounds [13]. For the case of the $LaSrMnNbO_6$ compound the higher intensity of the A-feature, relative to the B-feature, and chemical shift place its valence clearly in the Nb^{5+} range.

The complete ordering of Mn^{2+} and Nb^{5+} is thus expected, given the large differences of both charge (3) and cation size (Mn^{2+}: 0.83 Å and Nb^{5+}: 0.64 Å in octahedral coordination) [20]. As shown in Table 3, the Mn^{2+} and Nb^{5+} cations are located at the center of slightly distorted octahedra with average ⟨Mn–O⟩ and ⟨Nb–O⟩ distances of 1.99 and 2.15 Å, respectively. Corresponding to the low value of Goldschmid's tolerance factor: $t=\langle A\text{–}O\rangle/\sqrt{2}\langle B\text{–}O\rangle=0.905$, the octahedral framework is strongly distorted as indicated by the Mn–O–Nb bond angles (Table 3), which are much lower than 180°. The tilting angle of the $(Mn/Nb)O_6$ octahedra can be defined as $\varphi=(180-\phi)/2$, where ϕ is the Mn–O–Nb bond angle ($\phi=180°$ for the ideal cubic perovskite). From Table 3, the tilt angles can be calculated to be 13.38° [110], 12.20° [1–10] and 13.22° [001], in good agreement with the expected $a^-b^-c^+$ Glazer tilt system. The tilt angles of approximately 13°, signal a large deviation from the cubic perovskite structure; this is confirmed by the lowering of the La/Sr coordination from 12 to 8 (Table 3). The bond valence sum

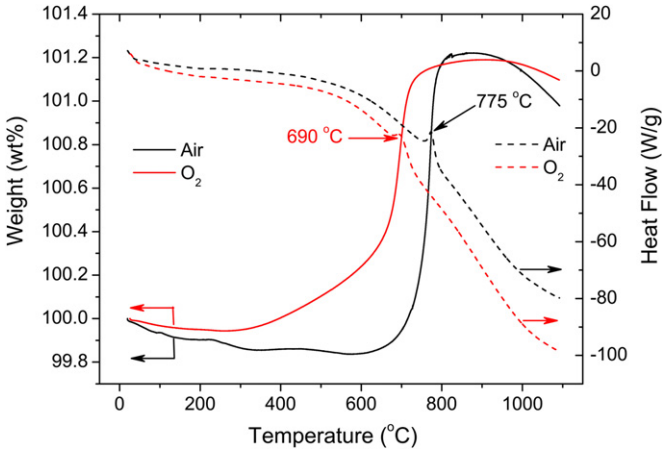

Fig. 4. Coupled TGA–DTA curves in air and O_2 atmospheres.

(BVS) values for the Mn^{2+} and Nb^{5+} cations of 2.25 and 4.99 (Table 2), respectively, are consistent with the nominal values.

In comparison to the reported Ca-analog $LaCaMnNbO_6$, [3] the ⟨Mn–O⟩ and ⟨Nb–O⟩ bonds are almost the same in the two compounds, but the ⟨A–O⟩ bond distance increases from 2.58 Å in the Ca-compound to 2.65 Å in the Sr-compound. As expected, the average Glazer tilt angle changes from ~16° to ~13° to compensate for the increasing average size of the A-cation in the Sr-analog. The tolerance factor increases from the Ca- to the Sr-analog from 0.88 to 0.905, and both phases are in the range where the $a^-b^-c^+$ ($P2_1/n$) tilt system is favored.

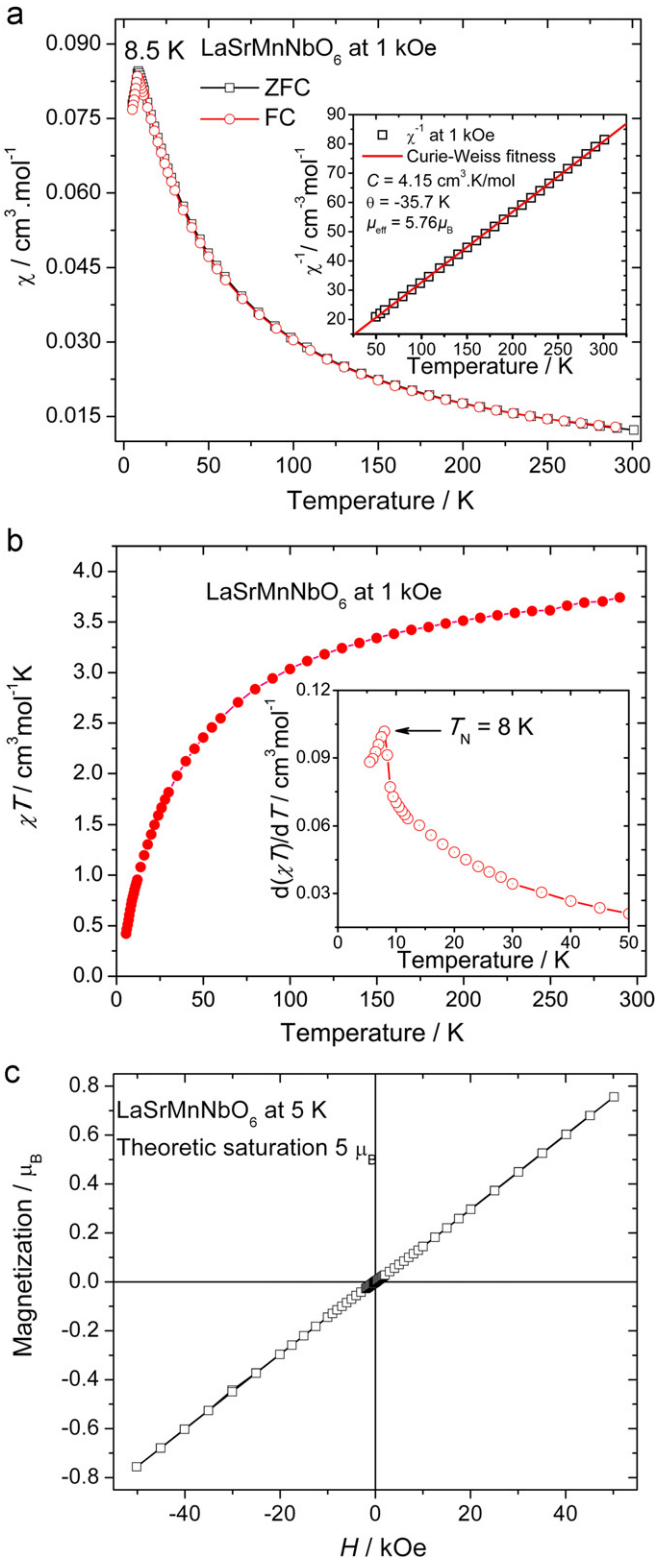

Fig. 5. (a) Magnetic susceptibilities $\chi(T)$ at 1 kOe field at ZFC and FC conditions for $LaSrMnNbO_6$. The inset is the *Curie–Weiss* fit of the reciprocal susceptibility χ^{-1} vs. T, (b) χT vs. T at 1 kOe at FC condition and the inset is the d(χT)/dT vs. T curve and (c) field dependence of the magnetization plot at 5 K.

LaSrMnNbO$_6$ is a metastable phase as seen in Fig. 4. TGA–DTA measurements in air and O_2 atmospheres up to 1100 °C both show a weight increase, accompanied by an exothermic peak at 775 and 690 °C, respectively. PXD patterns recorded after the TGA measurements (Fig. S2 in the Supporting Information) indicate that this weight change is due to decomposition, probably an oxidation reaction of Mn^{2+} to Mn^{3+}.

In the structure of LaSrMnNbO$_6$, the Mn^{2+} atoms are well separated by NbO_6 octahedra and can be considered as a 3D net with a shortest Mn^{2+}–Mn^{2+} distance of ~5.7 Å. Thus the magnetic interactions are mainly transmitted through O^{2-}–Nb^{5+}–O^{2-} three-ion-bridges, which is expected to be weak. With a polycrystalline sample, the temperature-dependent susceptibility has been measured in the range of 5–300 K at 1 kOe (Fig. 5a) and 1 T (Fig. S3 in the Supporting Information). The reciprocal susceptibility $\chi^{-1}(T)$ above 50 K follows the *Curie–Weiss* law reasonably well and yields C=4.15 cm^3 K mol^{-1} and θ=−35.7 K, as shown in the inset of Fig. 5a. The effective magnetic moment μ_{eff} can be estimated to be 5.76 μ_B, which is in good agreement with the spin only value calculated as $g\sqrt{S(S+1)}\,\mu_B$=5.9 μ_B, by assuming S=5/2 and g=2 for Mn^{2+}. The negative value of θ suggests the interactions between Mn^{2+} are mainly AFM, which is also supported by the monotonous decrease of χT in the whole temperature region (Fig. 5b). A cusp in the $\chi(T)$ plot at about 8.5 K suggests AFM long-range ordering. In addition, the zero field cooling (ZFC) and field cooling (FC) susceptibilities are identical as shown in Fig. 5a, confirming the AFM character. The ordering temperature T_N, estimated from the differential of the χT curve, is about 8.0 K (see the inset of Fig. 5b). The isothermal magnetization curve at 5 K (Fig. 5c) shows a linear increase up to 50 kOe with the value of 0.76 μ_B, which is ~15% of the theoretical saturation value (5 μ_B).

4. Conclusions

A new double perovskite LaSrMnNbO$_6$ has been synthesized by high temperature solid state reaction in 1% H_2/Ar dynamic flow. The structure was determined by Rietveld refinement of the PXD data. LaSrMnNbO$_6$ crystallizes in the monoclinic space group $P2_1/n$, which was also confirmed by electron diffraction. The valence state of Mn was confirmed by XAS to be 2+. Thus, due to the large size and charge differences, Mn^{2+} and Nb^{5+} are almost completely ordered over the B-site (< 1% inversion). The octahedral framework displays a significant tilting distortion, $a^-b^-c^+$ according to Glazer's tilt system. Upon heating, LaSrMnNbO$_6$ decomposes at 690 °C under O_2 flow or at 775 °C in air. The magnetic susceptibility data indicate the presence of long-range antiferromagnetic ordering at T_N=8 K. The experimentally observed effective magnetic moment, μ_{eff}=5.76 μ_B is in good agreement with the calculated value (μ_{calcd}=5.92 μ_B) for high spin Mn^{2+} ($3d^5$, S=5/2).

Acknowledgment

This work was partially supported by NSF-DMR 0541911 grant (M.G., T.Y.). J.H. acknowledges financial support from the European Union under the Framework 6 program under a contract for an Integrated Infrastructure Initiative. Reference 026019 ESTEEM.

Appendix A. Supplementary Materials

Supplementary data associated with this article can be found in the online version at doi:10.1016/j.jssc.2010.08.041.

References

[1] P.K. Davies, H. Wu, A.Y. Borisevich, I.E. Molodetsky, L. Farber, Annu. Rev. Mater. Res. 38 (2008) 369–401 and references therein.
[2] R.A. Wheeler, M.H. Whangbo, T. Hughbanks, R. Hoffmann, J.K. Burdett, T.A. Albright, J. Am. Chem. Soc. 108 (1986) 2222–2236.
[3] K.M. Ok, P. Shiv Halasyamani, D. Casanova, M. Llunell, P. Alemany, S. Alvarez, Chem. Mater. 18 (2006) 3176–3183.
[4] J.G. Bos, J.P. Attfield, Z. Anorg. Allg. Chem. 630 (2004) 2248–2252.
[5] J.G. Bos, J.P. Attfield, Phys. Rev. B 70 (2004) 174434.
[6] TOPAS V2.1: General Profile and Structure Analysis Software for Powder Diffraction Data, Bruker AXS, Karlsruhe, Germany.
[7] M.T. Anderson, K.B. Greenwood, G.A. Taylor, K.R. Poeppelmeier, Prog. Solid State Chem. 22 (1993) 197–233.
[8] A.M. Glazer, Acta Crystallogr. B 28 (1972) 3384–3392.
[9] M. Croft, D. Sills, M. Greenblatt, C. Lee, S.W. Cheong, K.V. Ramanujachary, D. Tran, Phys. Rev. B 55 (1997) 8726–8732.
[10] G. Popov, M. Greenblatt, M. Croft, Phys. Rev. B 67 (2003) 024406.
[11] T.K. Mandal, V. Poltavets, M. Croft, M. Greenblatt, J. Solid State Chem. 181 (2008) 2325–2331.
[12] T.K. Mandal, M. Croft, J. Hadermann, G. Van Tendeloo, P.W. Stephens, M. Greenblatt, J. Mater. Chem. 19 (2009) 4382–4390.
[13] R.O. Bune, M.V. Lobanov, G. Popov, M. Greenblatt, C.E. Botez, P.W. Stephens, M. Croft, E.N. Caspi, A.M. Abakumov, J. Hadermann, G.Van Tendeloo, Chem. Mater. 18 (2006) 2611–2617.
[14] Z. Zeng, M. Croft, M. Greenblatt, Mater. Res. Bull. 36 (2001) 705–715.
[15] G.M. Veith, M. Greenblatt, M. Croft, J.B. Goodenough, Mater. Res. Bull. 36 (2001) 1521–1530.
[16] K.V. Ramanujschary, S.E. Lofland, W. McCarroll, T. Emge, M. Greenblatt, M. Croft, J. Solid State Chem. 164 (2002) 60–70.
[17] G.M. Veith, M.V. Lobanov, T.J. Emge, M. Greenblatt, M. Croft, F. Stowasser, J. Hadermann, G.Van Tendelo, J. Mater. Chem. 14 (2004) 1623–1630.
[18] G.M. Veith, M. Greenblatt, M. Croft, K.V. Ramanujachary, J. Hattrick-Simpers, S.E. Lofland, I. Nowik, Chem. Mater. 17 (2005) 2562–2567.
[19] Y.H. Huang, G. Liang, M. Croft, M. Lehtimaki, M. Karppinen, J.B. Goodenough, Chem. Mater. 21 (2009) 2319–2326.
[20] R.D. Shannon, Acta Crystallogr. A 32 (1976) 751–767.